3D Spectroscopy of Vibrational Coherences in Quantum Dots: Theory

ARTICLE *in* THE JOURNAL OF PHYSICAL CHEMISTRY B · APRIL 2013

Impact Factor: 3.3 · DOI: 10.1021/jp4011444 · Source: PubMed

3 AUTHORS, INCLUDING:

Thorsten Hansen
Lund University
25 PUBLICATIONS **522** CITATIONS
SEE PROFILE

Tönu Pullerits
Lund University
180 PUBLICATIONS **5,469** CITATIONS
SEE PROFILE

THE JOURNAL OF PHYSICAL CHEMISTRY B

Article

pubs.acs.org/JPCB

3D Spectroscopy of Vibrational Coherences in Quantum Dots: Theory

Joachim Seibt,* Thorsten Hansen, and Tõnu Pullerits

Department of Chemical Physics, Lund University, Box 124, SE-21000, Lund, Sweden

ABSTRACT: In semiconductor nanocrystals, called quantum dots (QD), electronic transition energies, phonon frequencies, and electron−phonon coupling strengths are all reported to depend on the size of the crystals. The size dependencies of the transition energies and the mode frequencies are well characterized and understood. At the same time, the electron-phonon coupling dependence on size is controversial—even the sign of the change is not settled. In this article, third-order response functions of a model QD resembling CdSe are calculated. The longitudinal optical (LO) mode is included as a relatively narrow Lorentzian contribution to the spectral density. A novel version of electronic 2D spectroscopy is investigated where a third Fourier transform is taken over a so-called population time, leading to 3D spectral representation. The amplitude and phase of the 2D cuts of the 3D spectral body around the LO mode frequency are analyzed. The analytical power and sensitivity of the cuts in determining the possible Huang−Rhys factor (electron-phonon coupling strength) and the LO mode frequency dependence on the QD size are investigated. Peak structures in the cuts with a tilt relative to the diagonal are identified as sensitive signatures for the size dependencies. The study elucidates the 3D representation of the electronic 2D spectroscopy as a powerful tool for obtaining insight into otherwise hardly accessible characteristics of the system.

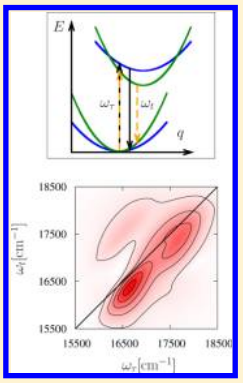

INTRODUCTION

Two-dimensional spectroscopy in the optical spectral range is an established tool for a comprehensive investigation of the ultrafast photoinduced dynamics. Experimental methodology and theoretical concepts of this technique have been discussed extensively in previous publications.[1−11] 2D spectra of a dimer system were analyzed in terms of contributions from different response functions[12,13] and Liouville space pathways including either populations or coherences between the exciton states. The relevance of the phase in 2D electronic spectroscopy was pointed out in the context of the time evolution of peak intensities, where a phase shift of about 90° was interpreted as quantum transport, i.e., excitation transfer between coherences and populations.[14] The influence of vibrations on the relative phase between the time evolution of different peaks in the 2D spectrum of a molecular dimer was discussed recently,[15] extending a previous approach where the origin of long-lived coherences was attributed to vibrational effects.[16] Furthermore, the role of the phase in 2D spectroscopy for the distinction between electronic and vibrational coherences was investigated.[17] Here we concentrate on the question if or to which extent an additional Fourier transformation with respect to a third pulse delay variable and the evaluation of both amplitude and phase at a selected position with respect to the corresponding frequency axis gives more insight into system properties than a usual 2D spectrum. Various versions of three-dimensional spectroscopy have previously been applied via fifth-order processes in the infrared[18] and visible[19] and via third-order processes in the visible spectral range.[20] We aim to draw a connection between the photophysical properties of CdSe quantum dots and features in coherent multidimensional spectroscopy. Our approach is based on the reported dependence of vibrational frequency, Huang−Rhys factor, and electronic excitation energy on the CdSe quantum dot size.[21−24] Vibrational frequencies and the corresponding Huang−Rhys factors determine the spectral density of the electron−phonon coupling—the key element of any microscopic transport description.[25] Our work is directly motivated by the potential of QDs as light harvesting materials in devices like QD sensitized solar cells.[26,27] Such devices borrow many ideas from photosynthesis; for example, the light absorbing part (antenna/QD) and electron transport part (reaction center/ZnO) are clearly separated.[28] CdSe QDs have been studied by electronic 2D spectroscopy.[29] The work mainly discusses electronic coherences and dephasing but reports even beating which is closely related to the LO mode. Since the appearance of vibrational modes in coherent multidimensional spectroscopy has recently received considerable attention,[15−17,30] we here present comprehensive simulation of vibrational effects in electronic 2D spectroscopy of quantum dots. We pay specific attention to the explanation of the effect of a tilt of peak structures in the two-dimensional spectrum taken at a fixed position with respect to the third frequency variable. Additionally, we give an interpretation of the phase in terms of resonance phenomena.[31] With our investigation, we demonstrate how to interpret two-dimensional cuts of measured 3D spectra in terms of a dependence of vibrational frequency and Huang−Rhys factor on the distributed particle size. The paper

Special Issue: Rienk van Grondelle Festschrift

Received: January 31, 2013
Revised: March 12, 2013
Published: April 5, 2013

   dx.doi.org/10.1021/jp4011444 | J. Phys. Chem. B 2013, 117, 11124−11133

is organized as follows: In the Introduction, we present the model system with attention to the aspect of how vibrations are treated using line shape functions and how they enter in the response functions from which the 3D spectrum is obtained. Furthermore, we specify the parameters used for the calculation. In the discussion of the results, we first consider the line shape functions which appear in the calculations. Then, we present 2D spectra with resolution of the vibrational substructure in distinction to 3D spectra. Finally, we give an interpretation of the appearing peak tilt feature in two-dimensional cuts of 3D spectra taken near the vibrational frequency. We discuss our findings in terms of the quantum dot size dependence of vibrational frequency and Huang–Rhys factor and summarize them in the conclusions.

THEORETICAL METHODS

Model System. Even though we include vibrational effects in the form of contributions to the spectral density of an environment by using line shape functions, we choose the concept of potential curves for an illustrative description. In Figure 1, harmonic potentials of all electronic states included in the model are shown together with the feasible optical transitions.

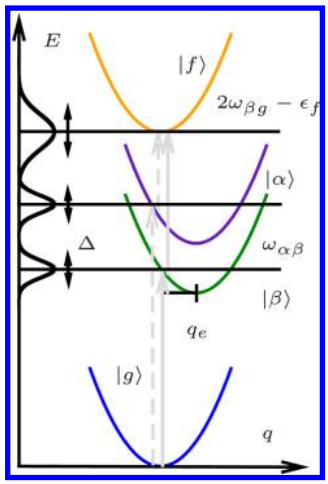

Figure 1. Energy diagram of the electronic states $|g\rangle$, $|\alpha\rangle$, $|\beta\rangle$, and $|f\rangle$ included in the model. The vibrational oscillations upon electronic excitations are indicated in terms of harmonic potentials. The energetic position of the singly excited state potentials and the doubly excited state potential are varied by a parameter Δ with a Gaussian distribution. Electronic transitions, which can take place between the electronic ground state and a singly excited state or between a singly excited state and the doubly excited state, are represented by gray arrows.

Besides the electronic ground state $|g\rangle$, we include the singly excited states $|\alpha\rangle$ and $|\beta\rangle$ and the doubly excited state $|f\rangle$. Between the states $|\alpha\rangle$ and $|\beta\rangle$, an energy gap $\omega_{\alpha\beta} = \omega_{\alpha g} - \omega_{\beta g} > 0$ appears, where $\omega_{\alpha g}$ and $\omega_{\beta g}$ denote the vertical transition energies from the electronic ground state to the states $|\alpha\rangle$ and $|\beta\rangle$. The averaged energy of the singly excited states $\omega_{eg} = {}^1/_2(\omega_{\alpha g} + \omega_{\beta g})$ can be taken as a reference energy if the rotating wave approximation is used. The energetic position of the doubly excited state corresponds to $2\omega_{\beta g} - \varepsilon_f$, where ε_f can be identified with the binding energy of the doubly excited state.[32] To account for static disorder, the levels can be shifted in energy by varying a parameter Δ. The equilibrium positions of the potentials of ground state and singly excited state are displaced relative to each other by q_e, and the same holds for the relative position of the minima of singly and doubly excited state potentials. The vibrational degree of freedom, which is characterized by the central frequency $\omega_{0,L}$, the Huang–Rhys factor $S_{L,i}$ with $i \in \{\alpha, \beta, f\}$, and the damping constant γ_L, accounts for the longitudinal optical (LO) mode of the quantum dots.

It enters as a Lorentzian contribution to the spectral density.[33] The respective spectral density reads[34]

$$J_{L,i} = \frac{2^{3/2} S_{L,i} \omega_{0,L}{}^3 \gamma_L \omega}{(\omega^2 - \omega_{0,L}{}^2)^2 + 2\gamma_L{}^2 \omega^2}, \quad i \in \{\alpha, \beta, f\} \tag{1}$$

In the case of $i \in \{\alpha, \beta\}$, the Huang–Rhys factor corresponds to $S_{L,\alpha} = S_{L,\beta} = {}^1/_2 q_e{}^2$. Acoustic phonons are included in the model in the form of a Debye contribution to the spectral density,[12] which is characterized by the Huang–Rhys-factor S_D and cutoff frequency ω_c. We use the modified expression

$$J_D = 2\pi S_D \operatorname{sgn}(\omega) \frac{\omega^4}{2\omega_c{}^3} \exp\left(-\frac{\omega}{\omega_c}\right) \tag{2}$$

The decay of populations and the lifetime broadening of coherences due to relaxation processes[35] enter in terms of phenomenological rates in our model, which allow the influence of additional electronic states to be included. A detailed discussion of the transfer processes which are included here can be found in the literature.[36−38] The line shape functions which also account for pure dephasing effects are obtained according to the formula[39]

$$g(t) = \frac{1}{2\pi} \int_{-\infty}^{\infty} d\omega \frac{1 - \cos(\omega t)}{\omega^2} \coth\left(\frac{\omega}{2k_B T}\right) J(\omega) + \frac{i}{2\pi} \int_{-\infty}^{\infty} d\omega \frac{\sin(\omega t) - \omega t}{\omega^2} J(\omega) \tag{3}$$

In general, the line shape functions are related to the electronic states in which the respective time evolution takes place and depend on the specific spectral densities related to these states.[6] Furthermore, it plays a role if or to which extent the fluctuations at the different electronic states are correlated,[32] as the line shape function is connected to the correlation function

$$C(t) = \int_{-\infty}^{\infty} d\omega \cos(\omega t) \coth\left(\frac{\omega}{2k_B T}\right) J(\omega) + i \int_{-\infty}^{\infty} d\omega \sin(\omega t) J(\omega) \tag{4}$$

via

$$g(t) = \frac{1}{2\pi} \int_0^t d\tau_1 \int_0^{\tau_1} d\tau_2 C(\tau_2) \tag{5}$$

For the calculation of 2D spectra, we use a perturbative description based on the response functions. The time intervals between the electronic excitations are denoted as t_1, t_2, and t_3.

As the size of the nanoparticles is distributed in a sample and the electronic excitation depends on the particle size,[23] we take the size distribution into account in terms of a Gaussian distribution of a parameter Δ with standard deviation σ_Δ. This parameter accounts for a shift in the electronic excitation energy in the singly excited states. Under the assumption that

dx.doi.org/10.1021/jp4011444 | J. Phys. Chem. B 2013, 117, 11124−11133

the energies of both electronic states depend on the particle size in the same way, we consider the energy shifts of both singly excited states to be equal (see Figure 1). To include also the size dependence[23,40] of $\omega_{0,L}$ and S_L, we take a functional dependence of these quantities on Δ into account. The contributions to the 2D spectrum arise from Fourier transformation of the response functions[6,41]

$$R_{1g}(t_1, t_2, t_3) = \sum_{\{kl\}\in\{\alpha,\beta\}} \frac{1}{(2\pi{\sigma_\Delta}^2)^{1/2}} \int_{-\infty}^{\infty} d\Delta e^{-\Delta^2/2{\sigma_\Delta}^2} \times e^{-i((\omega_{kg}+\Delta)-\omega_{eg})t_1 - i((\omega_{kg}+\Delta)-(\omega_{lg}+\Delta))t_2 - i((\omega_{kg}+\Delta)-\omega_{eg})t_3} \times e^{-(1/2)\Gamma_k t_1 - (\Gamma_k+\Gamma_l)((1/2)\delta_{kl}+(1/2)(1-\delta_{kl}))t_2 - (1/2)\Gamma_k t_3} \times e^{-g_{kl}(t_1) - g_{kk}^*(t_2) - g_{kl}^*(t_3) + g_{kl}(t_1+t_2) + g_{kl}^*(t_2+t_3) - g_{ll}(t_1+t_2+t_3)} \quad (6)$$

$$R_{2g}(t_1, t_2, t_3) = \sum_{\{kl\}\in\{\alpha,\beta\}} \frac{1}{(2\pi{\sigma_\Delta}^2)^{1/2}} \int_{-\infty}^{\infty} d\Delta e^{-\Delta^2/2{\sigma_\Delta}^2} \times e^{i((\omega_{kg}+\Delta)-\omega_{eg})t_1 - i((\omega_{lg}+\Delta)-(\omega_{kg}+\Delta))t_2 - i((\omega_{lg}+\Delta)-\omega_{eg})t_3} \times e^{-(1/2)\Gamma_k t_1 - (\Gamma_k+\Gamma_l)((1/2)\delta_{kl}+(1/2)(1-\delta_{kl}))t_2 - (1/2)\Gamma_l t_3} \times e^{-g_{kl}^*(t_1) + g_{kl}(t_2) - g_{kl}^*(t_3) - g_{ll}^*(t_1+t_2) - g_{kk}(t_2+t_3) + g_{kl}^*(t_1+t_2+t_3)} \quad (7)$$

$$R_{3g}(t_1, t_2, t_3) = \sum_{\{kl\}\in\{\alpha,\beta\}} \frac{1}{(2\pi{\sigma_\Delta}^2)^{1/2}} \int_{-\infty}^{\infty} d\Delta e^{-\Delta^2/2{\sigma_\Delta}^2} \times e^{i((\omega_{kg}+\Delta)-\omega_{eg})t_1 - i((\omega_{lg}+\Delta)-\omega_{eg})t_3} \times e^{-(1/2)\Gamma_k t_1 - (1/2)\Gamma_l t_3} \times e^{-g_{ll}^*(t_1) + g_{kl}^*(t_2) - g_{kk}(t_3) - g_{kl}^*(t_1+t_2) - g_{kl}^*(t_2+t_3) + g_{kl}^*(t_1+t_2+t_3)} \quad (8)$$

$$R_{4g}(t_1, t_2, t_3) = \sum_{\{kl\}\in\{\alpha,\beta\}} \frac{1}{(2\pi{\sigma_\Delta}^2)^{1/2}} \int_{-\infty}^{\infty} d\Delta e^{-\Delta^2/2{\sigma_\Delta}^2} \times e^{-i((\omega_{kg}+\Delta)-\omega_{eg})t_1 - i((\omega_{lg}+\Delta)-\omega_{eg})t_3} \times e^{-(1/2)\Gamma_k t_1 - (1/2)\Gamma_l t_3} \times e^{-g_{ll}(t_1) - g_{kl}(t_2) - g_{kk}(t_3) + g_{kl}(t_1+t_2) + g_{kl}(t_2+t_3) - g_{kl}(t_1+t_2+t_3)} \quad (9)$$

$$R_{1f}^*(t_1, t_2, t_3) = \sum_{\{kl\}\in\{\alpha,\beta\}} \frac{1}{(2\pi{\sigma_\Delta}^2)^{1/2}} \int_{-\infty}^{\infty} d\Delta e^{-\Delta^2/2{\sigma_\Delta}^2} \times e^{i((\omega_{kg}+\Delta)-\omega_{eg})t_1 + i((\omega_{kg}+\Delta)-(\omega_{lg}+\Delta))t_2 + i((\omega_{kg}+\Delta)-\varepsilon_f+(1/2)\omega_{\alpha\beta}-\omega_{eg})t_3} \times e^{-(1/2)\Gamma_k t_1 - (\Gamma_k+\Gamma_l)((1/2)\delta_{kl}+(1/2)(1-\delta_{kl}))t_2 - (1/2)\Gamma_k t_3} \times e^{-g_{kl}^*(t_1) - g_{ll}(t_2) - g_{kl}(t_3) + g_{kl}^*(t_1+t_2) + g_{kl}(t_2+t_3) - g_{kk}^*(t_1+t_2+t_3)} \times e^{+g_{lf}(t_2) + g_{lf}(t_3) - g_{kf}(t_3) - g_{kf}^*(t_1+t_2) - g_{lf}(t_2+t_3) + g_{kf}^*(t_1+t_2+t_3)} \times e^{-g_{ff}(t_3)} \quad (10)$$

$$R_{2f}^*(t_1, t_2, t_3) = \sum_{\{kl\}\in\{\alpha,\beta\}} \frac{1}{(2\pi{\sigma_\Delta}^2)^{1/2}} \int_{-\infty}^{\infty} d\Delta e^{-\Delta^2/2{\sigma_\Delta}^2} \times e^{-i((\omega_{kg}+\Delta)-\omega_{eg})t_1 - i((\omega_{kg}+\Delta)-(\omega_{lg}+\Delta))t_2 + i((\omega_{lg}+\Delta)-\varepsilon_f+(1/2)\omega_{\alpha\beta}-\omega_{eg})t_3} \times e^{-(1/2)\Gamma_k t_1 - (\Gamma_k+\Gamma_l)((1/2)\delta_{kl}+(1/2)(1-\delta_{kl}))t_2 - (1/2)\Gamma_l t_3} \times e^{-g_{kl}(t_1) + g_{kl}^*(t_2) - g_{kl}(t_3) - g_{ll}(t_1+t_2) - g_{kk}^*(t_2+t_3) + g_{kl}(t_1+t_2+t_3)} \times e^{-g_{kf}^*(t_2) + g_{lf}(t_3) + g_{kf}(t_3) + g_{lf}(t_1+t_2) + g_{kf}^*(t_2+t_3) - g_{lf}(t_1+t_2+t_3) - g_{ff}(t_3)} \quad (11)$$

R_{3g} and R_{4g} describe ground state bleaching (GSB), R_{1g} and R_{2g} account for stimulated emission (SE), and R_{1f}^* and R_{2f}^* are related to excited state absorption (ESA). Note that Δ enters as a parameter in the line shape functions if the central frequency and Huang–Rhys factor in the Lorentzian spectral density are functions of Δ. As we assume δ-shaped pulses, the time intervals t_1, t_2, and t_3 between the instantaneous excitations can be identified with the delay times τ, T, and t between the pulses after a convolution of the response functions with the pulses. Under the assumption of a fixed detection direction $k_s = -k_1 + k_2 + k_3$, the sign of the coherence time τ depends on whether pulse 1 with contribution $-k_1$ or pulse 2 with contribution k_2 to the detection direction arrives first. The population time T denotes the delay between pulse 2 and pulse 3, where the latter yields the contribution k_3 to the detection direction. The detection time t measures the interval from the arrival of pulse 3 up to the detection of the signal. Nonvanishing convolution integrals only appear for a pulse sequence 1−2−3 in the case of nonrephasing and for a pulse sequence 2−1−3 in the case of rephasing response functions. The formulas for the calculation of the 2D spectrum with respect to the time variables t_1 and t_3 read

$$\sigma_{2D,R}(\omega_\tau, t_2, \omega_t) = \int_0^\infty dt_1 \int_0^\infty dt_3 \exp(-i\omega_\tau t_1) \times \exp(i\omega_t t_3) P_R^{(3)}(t_1, t_2, t_3) \quad (12)$$

or

$$\sigma_{2D,NR}(\omega_\tau, t_2, \omega_t) = \int_0^\infty dt_1 \int_0^\infty dt_3 \exp(i\omega_\tau t_1) \times \exp(i\omega_t t_3) P_{NR}^{(3)}(t_1, t_2, t_3) \quad (13)$$

depending on whether rephasing ($P_R^{(3)}(t_1, t_2, t_3)$) or nonrephasing ($P_{NR}^{(3)}(t_1, t_2, t_3)$) contributions are considered.[1] In the case of δ-shaped pulses, the third-order polarizations $P_R^{(3)}$ and $P_{NR}^{(3)}$ can be identified with the third-order response consisting of the respective response function contributions:

$$P_R^{(3)}(t_1, t_2, t_3) = R_{2g}(t_1, t_2, t_3) + R_{3g}(t_1, t_2, t_3) - R_{1f}^*(t_1, t_2, t_3) \quad (14)$$

and

$$P_{NR}^{(3)}(t_1, t_2, t_3) = R_{1g}(t_1, t_2, t_3) + R_{4g}(t_1, t_2, t_3) - R_{2f}^*(t_1, t_2, t_3) \quad (15)$$

after convolution with the pulses, where in the case of δ-shaped pulses third-order polarizations and third-order responses are equivalent. Note that after application of eqs 12 and 13 there is still a parametric dependence on the delay time t_2 after the two-dimensional Fourier transformation. An additional Fourier transformation step with respect to t_2

$$\sigma_{3D}(\omega_\tau, \omega_T, \omega_t) = \int_0^\infty dt_2 \exp(-i\omega_T t_2) \sigma_{2D}(\omega_\tau, t_2, \omega_t) \quad (16)$$

allows for a further analysis. In order to consider only components which are related to oscillations with frequency ω_0 during the population time, a slice $\sigma_{3D}(\omega_\tau, \omega_T = \omega_0, \omega_t)$ is taken.

Population decay and lifetime broadening effects stemming from relaxation processes are taken into account in eqs 6−11, whereas additional Liouville space pathways due to population transfer are neglected. According to ref 41, these additional Liouville space pathways do not depend on the time variable t_2, so that their contribution at $\omega_T = 200\ cm^{-1}$ is negligible.

By representing the complex 2D spectrum as $\sigma_{3D} = A(\sigma_{3D}(\omega_\tau, \omega_T, \omega_t)) \exp(i\phi(\sigma_{3D}(\omega_\tau, \omega_T, \omega_t)))$, one obtains the amplitude $A(\sigma_{3D}(\omega_\tau, \omega_T, \omega_t))$ and the phase $\phi(\sigma_{3D}(\omega_\tau, \omega_T, \omega_t))$. Under simplifying assumptions in the case of rephasing contributions, the phase $\phi(\sigma_{3D,R}(\omega_\tau, \omega_T, \omega_t))$ can be interpreted as the difference of the phases which appear when the system evolves during the time intervals τ and t. The

dx.doi.org/10.1021/jp4011444 | J. Phys. Chem. B 2013, 117, 11124−11133

respective phases depend on the difference between the transition frequency and the relative energetic position of the electronic states as well as on the deviation of the vibrational oscillation from the resonance frequency due to vibrational relaxation. The latter aspect is related to resonance phenomena of an oscillator with a Lorentzian resonance profile centered at frequency $\omega_{0,L}$ and with damping constant γ_L.[31]

Choice of Parameters. The parameters of the model summarized in Table 1 are chosen to mimic CdSe nanocrystals.

Table 1. Numerical Values of the Parameters Entering in the Model

$\omega_{\beta g}$		$\omega_{\alpha g}$	ε_f
1.65×10^4 cm^{-1}		1.75×10^4 cm^{-1}	-650 cm^{-1}
$S_{L,\alpha} = S_{L,\beta}$	$S_{L,f}$	$\omega_{0,L}$	γ_L
0.2	0.0	200 cm^{-1}	25 cm^{-1}
S_D	ω_c	$t_{2,max}$	dt_2
0.11	25 cm^{-1}	8 ps	16 fs
Γ_α	k_BT	ω_0	FWHM(Δ)
30 cm^{-1}	200 cm^{-1}	200 cm^{-1}	800 cm^{-1}

The excitation energies from the electronic ground state to the singly excited states $\omega_{\beta g}$ and $\omega_{\alpha g}$ are located in the yellow region of the optical spectral range, and they are more than 1 order of magnitude larger than the splitting between them and the parameter ε_f for the energetic shift of the doubly excited state compared to the sum of the singly excited state electronic excitation energies relative to the ground state. For the choice of the Huang–Rhys factor entering in the Lorentzian spectral density as $S_{L,\alpha} = S_{L,\beta} = 0.2$ for transitions between ground and singly excited states, we take results from the literature[21] into account and assume that the doubly excited state is not displaced relative to the ground state by setting $S_{L,f}$ to zero. This choice is arbitrary. If the Huang–Rhys factor of the doubly excited state would be increased, the contribution from ESA processes to the intensity of the peaks appearing in two-dimensional cuts of the rephasing 3D spectra would be larger. Thereby the assumption of uncorrelated fluctuations leads to a leveling effect. Particularly in the case that the Huang–Rhys factors of singly and doubly excited states are equal, uncorrelated fluctuations keep the ESA peaks from becoming extremely narrow with respect to the ω_t-axis and so large in intensity that they would overgrow all other contributions. Note that the latter assumptions lead to a displacement between singly and doubly excited states, as the Huang–Rhys factor of the doubly excited state is related to the electronic ground state. The average vibrational frequency $\omega_{0,L}$ from the literature[23] and the damping constant $\gamma_L = 25$ cm^{-1} enter in the Lorentzian spectral density contribution. In the Debye contribution to the spectral density, we choose the reported value[21] of the Huang–Rhys factor S_D and fix the value of the cutoff frequency ω_c in a way that the position of the maximum of the Debye spectral density with inverse energy dimension,[42] i.e., eq 2 divided by $2\pi\omega^2$, is located at 50 cm^{-1} in agreement with experimental findings. The upper border $t_{2,max}$ of t_2 needs to be large enough to allow for a complete damping of the vibrations in order to make $\sigma_{3D}(\omega_\tau, \omega_T = \omega_0, \omega_t)$ converge. This condition is fulfilled for $t_{2,max} > 2$ ps, where the correlation function has almost completely decayed (see the Results and Discussion). The step size dt_2 determines the covered spectral range, which is subject to the condition that it comprises at least the energies up to the energy difference between the singly excited states $\omega_{\alpha\beta}$. As the covered spectral range is proportional to the inverse step size, the condition $dt_2 \leq 16$ fs is required. Our choice of values for $t_{2,max}$ in the order of 8 ps and for dt_2 in the order of 10 fs is appropriate to fulfill these conditions. Under the assumption of uncorrelated fluctuations, the line shape functions $g_{\alpha\beta}$, $g_{\beta\alpha}$, $g_{\alpha f}$, $g_{\beta f}$, $g_{f\alpha}$, and $g_{f\beta}$ and the corresponding correlation functions are equal to zero.[32] Consequently, the coherence terms in eqs 6–11 decay. The phenomenological rate constant Γ_α leads to a lifetime broadening with a time constant of about 200 fs. Dephasing times of this order of magnitude agree with the literature.[43] For the calculation of the line shape functions, we assume room temperature. We evaluate the 3D spectrum $\sigma_{3D}(\omega_\tau, \omega_T = \omega_0, \omega_t)$ at a fixed frequency ω_0, which corresponds to the average vibrational frequency. Under the assumption of Gaussian distribution with standard deviation σ_Δ, we vary Δ and thus shift the electronic energies of the singly excited states by the same amount. For the numerical integration over Δ, we take 80 steps within the interval borders from $-2\sigma_\Delta$ to $2\sigma_\Delta$ and study the effects of taking $\omega_{0,L}$ and S_L as functions of Δ in the following section.

RESULTS AND DISCUSSION

Line Shape Functions. Before we consider the calculated 2D spectra and two-dimensional slices of 3D spectra, we discuss the line shape functions entering in the response functions and the quantities they are calculated from. In Figure 2, the spectral densities according to eqs 1 and 2, the time correlation function (see eq 4), and the line shape function (see eq 5) are shown.

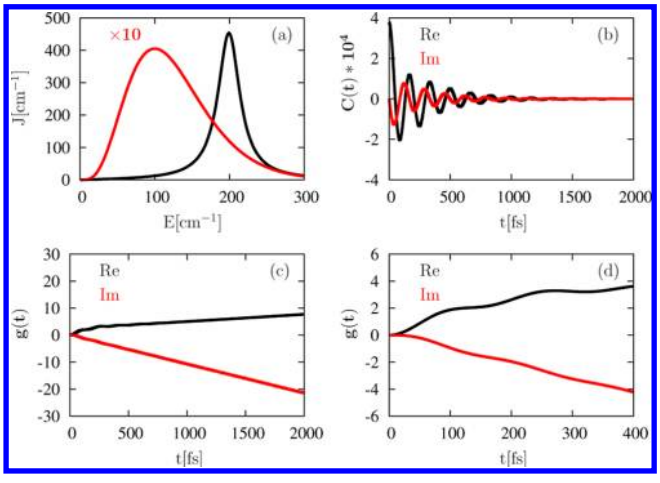

Figure 2. (a) Lorentzian (black line) and Debye (red line, multiplied by a factor of 10) contribution to the spectral density. (b) Correlation function (the real and imaginary parts correspond to the black and red curves, respectively). (c) Evolution of the line shape function during a long time interval (the real and imaginary parts correspond to the black and red curves, respectively). (d) Evolution of the line shape function during a short time interval.

While the Lorentzian spectral density contribution is relatively sharp, the Debye contribution is distributed over a much broader range of energies, but also much lower in intensity and therefore weighted by a factor of 10 in part a. Note that the Debye spectral density has its maximum at about 100 cm^{-1} upon multiplication with $2\pi\omega^2$, whereas without this factor it would appear at 50 cm^{-1}. The correlation function

dx.doi.org/10.1021/jp4011444 | J. Phys. Chem. B 2013, 117, 11124–11133

(part b) shows oscillations which can be assigned to the underdamped vibrational mode from the Lorentzian contribution to the spectral density. At about 2 ps, it has completely decayed. Both the real and imaginary parts of the line shape function (parts c and d) exhibit an approximately linear slope at longer times. At shorter times, an additional oscillatory component appears. In fluctuation−dissipation terminology, the real part of $g(t)$ originates from fluctuations and the imaginary part from dissipation.[44−46] In this way, the long time slopes of the real and imaginary parts of $g(t)$ correspond to the dephasing rate and frequency shift, respectively.

2D Spectra. 2D spectra from eqs 12 and 13 depend on the population time t_2. In Figure 3, the real and imaginary parts of 2D spectra of the rephasing response functions R_2, R_3, and R_1^* and their sum at t_2 = 8 ps are shown.

To make the vibrational substructure recognizable, the modified parameters $S_{L,\alpha} = S_{L,\beta} = 1$ and $\gamma_L = 5$ cm^{-1} were chosen, and inhomogeneous broadening was not taken into account by assuming the constant value $\Delta = 0$ cm^{-1}. Furthermore, relaxation was neglected by assuming $\Gamma_\alpha = 0$ cm^{-1}. Nevertheless, dephasing of electronic coherences still appears because of the assumption of uncorrelated fluctuations in different electronic states. The Feynman diagrams in Figure 4 show that in the case of the SE response function R_2

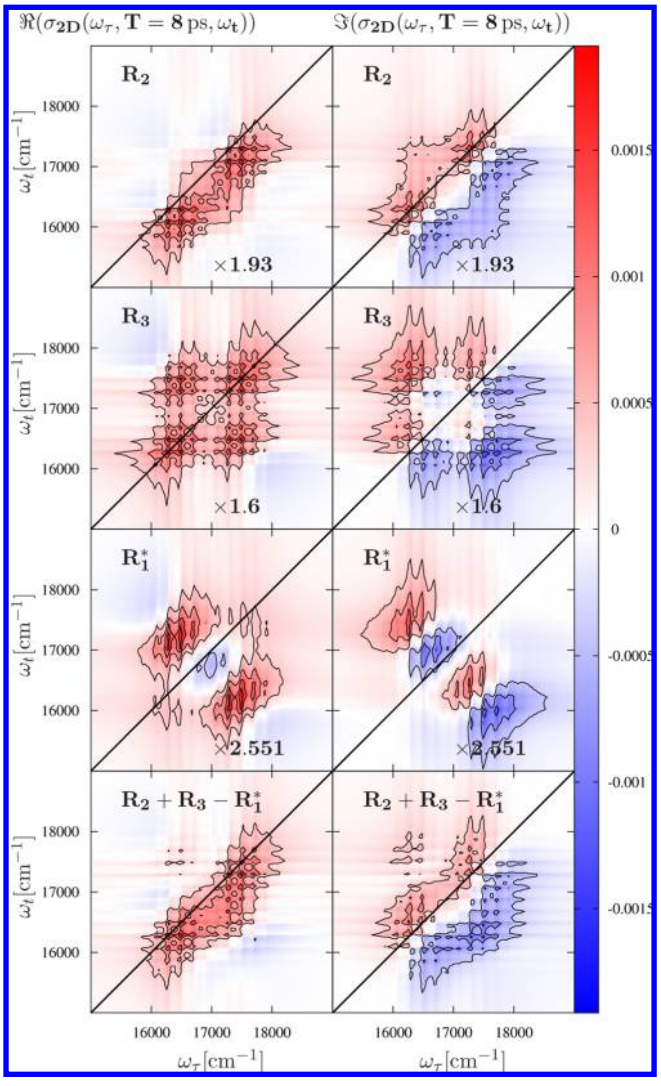

Figure 3. Real (left-hand side) and imaginary part (right-hand side) of 2D spectra of the rephasing response functions R_2, R_3, and R_1^* and their sum taken at t_2 = 8 ps. The calculation parameters are chosen in a way that allows a resolution of the vibrational substructure.

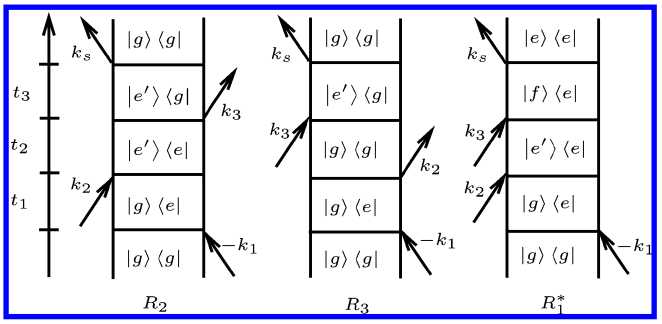

Figure 4. Feynman diagrams of the rephasing response functions R_2, R_3, and R_1^*. The singly excited state levels e and e′ can be identified with α or β, respectively.

evolution during t_2 takes place in the singly excited state, whereas in the case of the GSB response function R_3 a population of the electronic ground state appears during this interval.

In both R_2 and R_3 peak structures which stem from Liouville space pathways including only one of the singly excited states appear in the diagonal region. The appearance of different singly excited states in a Liouville space pathway leads to off-diagonal peak groups with lower intensity because of the dephasing of electronic coherences. In the case of R_2, the evolution during t_2 takes place in the subspace of the singly excited states, so that because of lifetime broadening the dephasing is larger than in the case of R_3, where the ground state is populated during t_2. All peaks from Liouville space pathways involving different electronic states show a vibrational substructure, where the spacing corresponds to the central frequency of the Lorentzian contribution to the spectral density. The 2D spectrum of R_1^* exhibits peak groups in the off-diagonal region which stem from Liouville space pathways with only one of the singly excited states involved. Also if both singly excited states are involved, the corresponding peak groups with their vibrational sub-structure appear in the off-diagonal region. Because of the assumption of uncorrelated fluctuations in singly and doubly excited states and the different Huang−Rhys factors, the ESA contribution plays a smaller role than those of SE and GSB in the rephasing 2D spectrum. Moreover, a detailed inspection of the 2D spectra shown in Figure 3 leads to the following findings: Because of the chosen value t_2 = 8 ps, which is large compared to the time constant corresponding to γ_L of about 200 fs, vibrational relaxation in the singly excited state can be considered as completed. Therefore, the vibrational features in the 2D spectrum of R_2 mainly appear below the diagonal. Using the picture of harmonic potentials for the description of the underlying processes, one can explain this effect by the shift between absorption and emission position coordinate, which leads to a modification of the potential difference and the corresponding transition frequency of the emission process relative to the absorption frequency.[47] In the case of R_3, the distribution of the vibrational peaks in the diagonal region above and below the diagonal is more balanced. In the imaginary part of R_2 and R_3, one finds that the nodal line defined by the sign change is aligned parallel to the diagonal and is thus parallel to the connecting line between the peak

dx.doi.org/10.1021/jp4011444 | J. Phys. Chem. B 2013, 117, 11124−11133

groups in the diagonal region. As the peak positions change along this line due to a shift of the electronic excitation energies of the singly excited states, constructive superposition effects appear if the parameter Δ varies. In the case of R_1^*, peaks from Liouville space pathways with singly excited state population are shifted depending on Δ along their antidiagonal connecting line, which is perpendicular to the nodal line defined by the sign change in the 2D spectrum. Therefore, destructive superposition effects appear in this case.

Two-Dimensional Cuts of 3D Spectra. If the parameters are set to the values defined in Table 1, the vibrational substructure of the peaks is not resolved anymore. In the results of the respective calculations shown in Figure 5, the influence of inhomogeneous broadening becomes recognizable because of the integration over the distribution of Δ.

Different from Figure 3, the amplitude and phase of two-dimensional cuts of 3D spectra at ω_T = 200 cm^{-1} are shown, which were calculated from the rephasing response functions R_2, R_3, and R_1^* and their sum. Thereby $\omega_{0,L}$ and $S_{L,\alpha} = S_{L,\beta}$ were taken as independent of Δ. The phase of the two-dimensional cuts shown in the column on the right-hand side of Figure 5 is encoded by the hue color scale, while the relative signal amplitude determines the intensity of the color at each point (ω_τ, ω_t). The peaks in the diagonal region of the two-dimensional cut of the complete rephasing 3D spectrum stem from the response functions R_2 and R_3, where the contribution of R_2 reflects the dynamics during the population time in the singly excited state. Because of relaxation processes which mainly affect the energetically higher singly excited state α, the lower diagonal peak in the contribution of R_2 is significantly more intensive than the upper one. The lower diagonal peak is elongated along the diagonal in the two-dimensional spectra of R_2 and R_3. This effect can be explained by constructive superposition of contributions from quantum dots with different sizes and therefore different electronic excitation energies. For R_2 and R_3, the gradient of the peak position with respect to the parameter Δ is perpendicular to the gradient of the phase, so that no cancellation effects appear. In the case of R_1^*, where this condition is not fulfilled, the peaks are much lower in intensity and not elongated in any certain direction.

In Figure 6, an illustration is given to explain the combined electronic and vibrational dynamics in the case of R_2 without considering the influence of inhomogeneous broadening.

After electronic excitation from the ground state to one of the singly excited states upon interaction with the first two pulses has taken place, subsequent vibrational oscillation of the population in β appears (see upper left panel). In the course of vibrational relaxation, the amplitude of oscillations decreases (see lower left panel and the orange curve in the upper right panel) and the phase shift relative to the initial oscillation increases (see upper right panel, red curve). Via the Fourier transformation with respect to t_2, each trajectory in Liouville space characterized by the transition frequencies and the corresponding absorption and emission position coordinate yields a contribution at the respective (ω_τ, ω_T, ω_t) position in the 3D spectrum with specific amplitude and phase. Both the size of the total amplitude value and the sum of the phases of contributions from different trajectories determine the peak intensity distribution. Because of a displacement of the singly excited state relative to the electronic ground state (quantified by $S_{L,\alpha} = S_{L,\beta}$), the transition frequency at the emission point becomes increasingly smaller than the transition frequency at the absorption point when the distance between absorption and

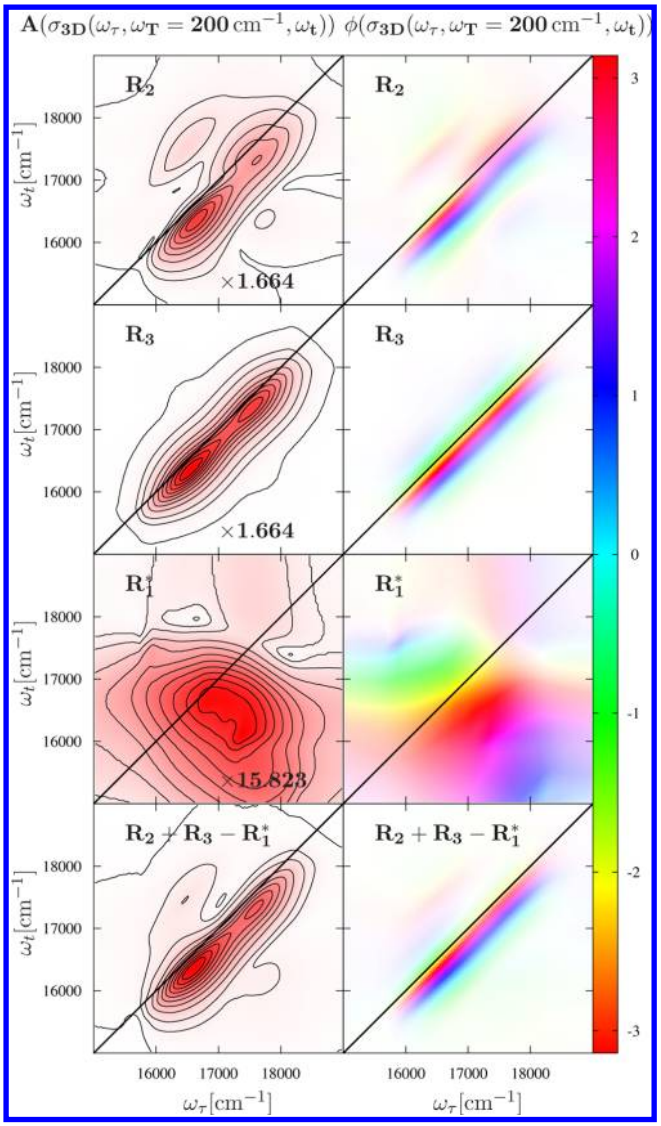

Figure 5. Amplitude (left-hand side) and phase (right-hand side) of two-dimensional cuts of the triple Fouier transformed rephasing response functions R_2, R_3, and R_1^* and their sum taken at ω_T = 200 cm^{-1}. The amplitude has only positive values. For each response function, a scaling factor to normalize the maxima of the amplitude with respect to the complete rephasing spectrum is given. In the 2D spectra on the right-hand side, the phase is encoded by the hue color scale represented by the color bar, while the relative amplitude determines the intensity of the color at each point.

emission point increases in the course of vibrational relaxation. If the Fourier component at the fixed frequency $\omega_T = \omega_0$ predominantly captures the evolution in the singly excited state at an advanced stage of the vibrational relaxation process, the corresponding peak in the two-dimensional cuts at the respective ω_T position of the 3D spectrum is located at a position with $\omega_\tau < \omega_t$ (see lower right panel).

The assumption of a Δ-dependent vibrational oscillation frequency $\omega_{0,L}$ leads to the results shown in Figure 7.

We assumed a linear dependence $\omega_{0,L}$ = 200 cm^{-1} − 0.0588∗Δ (i.e., a variation of $\omega_{0,L}$ between 240 and 160 cm^{-1} within the interval borders $-2\sigma_\Delta$ and $2\sigma_\Delta$). The tendency of a decreasing vibrational frequency with increasing parameter Δ agrees with the findings from the literature.[23] Both the electronic excitation energy and the vibrational frequency

dx.doi.org/10.1021/jp4011444 | J. Phys. Chem. B 2013, 117, 11124−11133

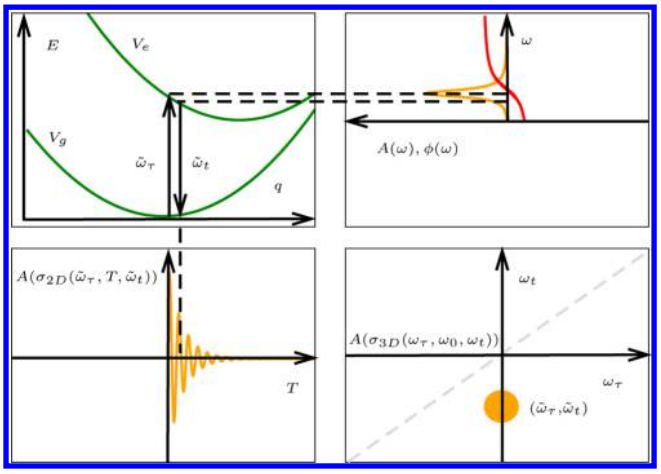

Figure 6. Upper left panel: Between the potentials of ground state and singly excited state β transitions appear with frequency $\tilde{\omega}_\tau$ at the absorption point and with frequency $\tilde{\omega}_t$ after vibrational relaxation has taken place to some extent during t_2. Lower left panel: The dependence of the amplitude of the 2D spectrum at $\tilde{\omega}_\tau$ and $\tilde{\omega}_t$ on the population time is shown, where the time dependence can be related to the progress of vibrational relaxation in the singly excited state subsequent to absorption. Upper right panel: Vibrational motion in the singly excited state is represented in terms of a Lorentzian oscillator characterized by amplitude (orange) and phase profile (red). Lower left panel: The two-dimensional cut taken at a fixed frequency $\omega_T = \omega_0$ after triple Fourier transformation is sketched. Thereby the origin of both the ω_τ- and ω_t-axis is chosen as the vertical transition energy. As a result of vibrational relaxation, the peak related to the excitation process from the upper left panel appears at a position with $\omega_t < \omega_\tau$.

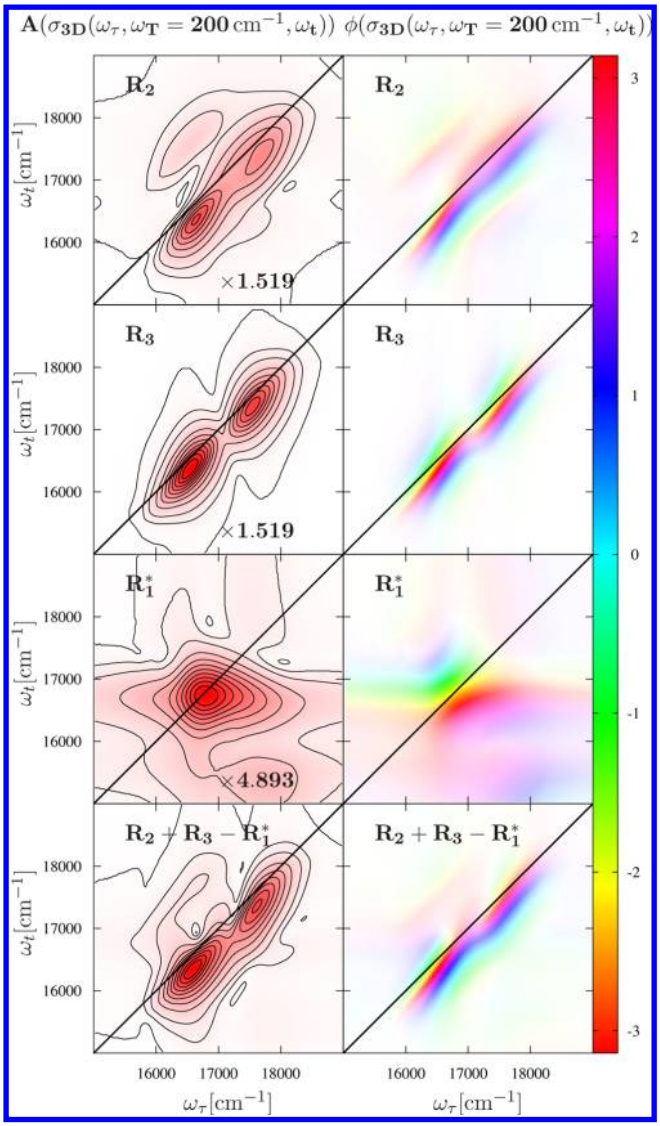

Figure 7. Amplitude (left-hand side) and phase (right-hand side) of two-dimensional cuts of the triple Fourier transformed rephasing response functions R_2, R_3, and R_1^* and their sum taken at $\omega_T = 200$ cm^{-1} (see also Figure 5). The oscillation frequency in Lorentzian spectral density is assumed to be a function of the shift of the electronic excitation energies compared to averaged levels.

depend on the particle size, where the first becomes larger with decreasing particle size, while the latter becomes smaller. In the two-dimensional cuts of 3D spectra of R_2 and R_3, the lower diagonal peak exhibits a tilt, which appears both in the amplitude and the phase. In the case of R_2, a tilt of the energetically higher diagonal peak is not clearly recognizable, particularly by considering the phase. The relaxation from the energetically higher to the lower singly excited state plays a role for this effect. Because of the population decay, signal contributions at small t_2 values relative to the time scale of relaxation gain a larger importance than those at larger values, which indicates that the tilt effect is mainly caused by the evolution at later times, i.e., not immediately after the absorption process. The crosspeak at $\omega_t > \omega_\tau$ in the two-dimensional cut at $\omega_T = \omega_0$ of R_2 is not tilted relative to the diagonal direction. This effect seems to be caused by the assumption of uncorrelated fluctuations, which makes the line shape functions with different indices in the respective response function vanish. As sketched above, in the case of R_2, the diagonal peaks exhibit a redshift of ω_t relative to ω_τ as a consequence of vibrational relaxation during the population time. This redshift depends on the difference of the potentials of the electronic states between which the electronic transitions take place at absorption and emission position coordinate. For different values of $\omega_{0,L}$, the slope of the potentials changes, so that the difference between them is modified even if the distance between absorption and emission position is unchanged (unless this difference is zero). However, also the extent of the tilt effect, which is clearly recognizable on the frequency scale of the displayed 2D spectra, suggests that also the weighting function of Liouville space trajectories with different distances between absorption and emission position depends on $\omega_{0,L}$. More precisely, the distribution of the Liouville space pathway contributions with different progress of vibrational relaxation parametrized by t_2 can be identified with the Fourier component at frequency $\omega_T = \omega_0$ given by the integral $\int_0^{t_2} dt_2' \exp(-i\omega_0 t_2')\sigma_{2D}(\omega_\tau, t_2', \omega_t)$. When this integral has converged, the upper border can be set to infinity and the expression for the third Fourier transformation is obtained.

A schematic illustration of the effect that in the case of a decrease of $\omega_{0,L}$ with the increasing parameter Δ the difference between absorption and emission frequency becomes larger at lower values of Δ is given in Figure 8.

There the potential curves of the ground state and the singly excited state β at two different electronic excitation energies are shown. While in the potential diagram on the left-hand side the potential curves are taken to be equal for different values of the electronic excitation energy, i.e., independent of Δ, on the right-hand side, the singly excited state potential with lower

dx.doi.org/10.1021/jp4011444 | J. Phys. Chem. B 2013, 117, 11124−11133

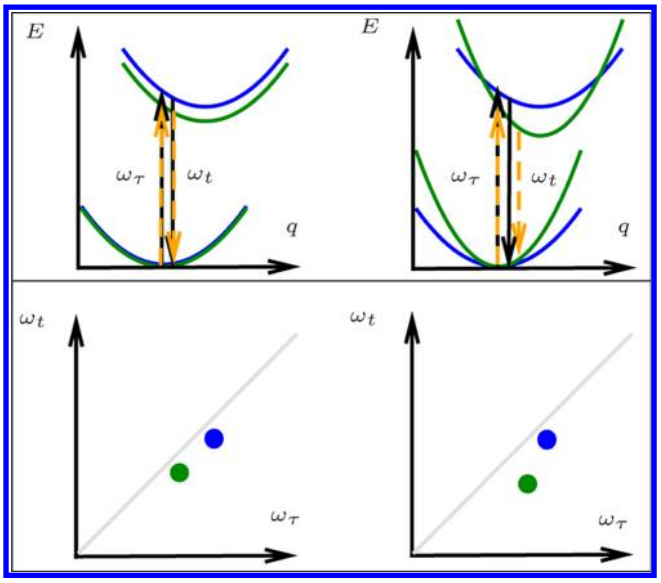

Figure 8. Illustration of the cases that the central vibrational frequency of the Lorentzian spectral density is independent of the electronic excitation energy (left-hand side) or depends on it (right-hand side). Below the potential diagrams, the resulting 2D spectra are sketched, where in the latter case with increasing absorption frequency ω_τ the emission frequency ω_t decreases.

energy at the absorption point exhibits a larger curvature corresponding to a larger vibrational frequency than the one of the energetically higher singly excited state potential. The dependence of the difference between the singly excited state and ground state potential on the vibrational coordinate results in a Δ-dependent redshift of the emission frequency relative to the absorption frequency as a result of vibrational relaxation during the waiting time.

The assumption that the Huang−Rhys factor depends on Δ as a linear function while the vibrational frequency is kept constant leads to a less pronounced tilt effect than in the case of a Δ-dependent vibrational frequency. For $S_{L,\alpha} = S_{L,\beta} = 0.2 - 2.941 \times 10^{-4}$ cm∗Δ (i.e., a variation of S_L between 0.4 and 0 justified by the values given in the literature[21] within the interval borders $-2\sigma_\Delta$ and $2\sigma_\Delta$), almost no tilt effect is recognizable. Therefore, the respective 2D spectra are not shown here. By assuming a steeper increase of the Huang−Rhys factor with decreasing value of Δ up to the unrealistic value of 0.8 at $-2\sigma_\Delta$, one finds that the peak structure in the lower diagonal region is tilted relative to the diagonal toward smaller ω_t values in the lower energy region. This tendency agrees with the findings for a Δ-dependent vibrational frequency, where we also assumed a negative gradient with respect to Δ. If both $\omega_{0,L}$ and S_L are assumed to become smaller with increasing value of Δ, the tilt effect is enhanced. In the literature, one finds contradictory results for the dependence of the Huang−Rhys factor on the particle size. A decrease with decreasing particle size[48] and thus with increasing value of Δ is reported as well as the opposite tendency.[24] In the latter case, the tilt appears in the opposite way compared to the previous case. Then, the higher energy region of the diagonal peaks structure is characterized by an increased redshift of ω_t compared to ω_τ. In combination with the opposite effect from the Δ-dependent vibrational frequency, compensation of the tilts can appear to some extent.

CONCLUSIONS

We have analyzed effects in amplitude and phase of two-dimensional cuts of rephasing 3D spectra taken at an energetic position near the frequency of a vibrational mode with respect to the frequency related to the population time. The model system was aimed to capture substantial spectroscopic properties of CdSe quantum dots. Four electronic states were taken into account with an internal vibration entering in terms of a Lorentzian contribution to the spectral density. We discussed the influence of a particle size distribution on parameters in the spectral density and on the distribution of electronic excitation energies. By constructive superposition effects, the latter leads to inhomogeneous broadening in terms of an elongation of the diagonal peaks from GSB and SE processes. In the case of ESA crosspeaks, destructive superposition of the signal contributions from quantum dots with different sizes appears. We found that an increase of the central oscillation frequency in the Lorentzian spectral density with the particle size is responsible for a tilt of the elongated diagonal peak structure relative to the diagonal. This effect is enhanced if the Huang−Rhys factor also shows the tendency to become larger with increasing particle size. In turn, from a tilt of the diagonal peak structure in results obtained from measurements, one can draw conclusions about the dependencies of vibrational frequency and Huang−Rhys factor on the particle size, which characterize the longitudinal optical phonon mode in the framework of our model. Furthermore, our investigations exemplify the interpretation of the amplitude and phase of two-dimensional cuts of 3D spectra. The phase taken at a certain frequency $\omega_T = \omega_0$ after Fourier transformation of the 2D spectra with respect to the waiting time can be considered as being composed of phase shifts during the delay times between the pulses or sums of them. For those phase shifts, it matters both whether an induced transition is resonant to the energy difference between the involved electronic states and how far vibrational relaxation during a certain time period drives the vibrational oscillation away from its resonance. The amplitude at a point (ω_τ, ω_t) of the 2D spectrum taken at $\omega_T = \omega_0$ corresponds to the superposition of contributions from Liouville space trajectories which include the respective combination of absorption frequency ω_τ and emission frequency ω_t. As a further step, the application of the presented theoretical description to a modified experimental technique, the fluorescence detected two-dimensional electronic coherence spectroscopy,[49] is planned. This technique allows a more detailed analysis of phase effects than standard 2D spectroscopy.

AUTHOR INFORMATION

Corresponding Author

*E-mail: Joachim.Seibt@chemphys.lu.se.

Notes

The authors declare no competing financial interest.

ACKNOWLEDGMENTS

We gratefully acknowledge financial support of the Knut and Alice Wallenberg Foundation, Crafoord Foundation, and Swedish Energy Agency. We thank Dr. Vytautas Butkus for the valuable discussions. Collaboration within nmC@LU is acknowledged.

REFERENCES

(1) Brixner, T.; Mančal, T.; Stiopkin, I. V.; Fleming, G. R. Phase-Stabilized Two-Dimensional Electronic Spectroscopy. *J. Chem. Phys.* **2004**, *121*, 4221−4236.

(2) Gallagher Faeder, S. M.; Jonas, D. M. Two-Dimensional Electronic Correlation and Relaxation Spectra: Theory and Model Calculations. *J. Phys. Chem. A* **1999**, *103*, 10489−10505.

(3) Cowan, M. L.; Ogilvie, J. P.; Miller, R. J. D. Two-dimensional Spectroscopy Using Diffractive Optics Based Phased-Locked Photon Echoes. *Chem. Phys. Lett.* **2004**, *386*, 184−189.

(4) Read, E. L.; Schlau-Cohen, G. S.; Engel, G. S.; Wen, J.; Blankenship, R. E.; Fleming, G. R. Visualization of Excitonic Structure in the Fenna-Matthews-Olson Photosynthetic Complex by Polarization-Dependent Two-Dimensional Electronic Spectroscopy. *Biophys. J.* **2008**, *95*, 847−856.

(5) Cheng, Y.-C.; Fleming, G. R. Coherence Quantum Beats in Two-Dimensional Electronic Spectroscopy. *J. Phys. Chem. A* **2008**, *112*, 4254−4260.

(6) Mukamel, S.; Abramavicius, D. Many-Body Approaches for Simulating Coherent Nonlinear Spectroscopies of Electronic and Vibrational Excitons. *Chem. Rev.* **2004**, *104*, 2073−2098.

(7) Brüggemann, B.; Pullerits, T. Nonperturbative Modeling of Fifth-Order Coherent Multidimensional Spectroscopy in Light Harvesting Antennas. *New J. Phys.* **2011**, *13*, 025024-1−025024-12.

(8) Brüggemann, B.; Kjellberg, P.; Pullerits, T. Non-Perturbative Calculation of 2D Spectra in Heterogeneous Systems: Exciton Relaxation in the FMO Complex. *Chem. Phys. Lett.* **2007**, *444*, 192−196.

(9) Egorova, D.; Gelin, M. F.; Domcke, W. Analysis of Cross Peaks in Two-Dimensional Electronic Photon-Echo Spectroscopy for Simple Models with Vibrations and Dissipation. *J. Chem. Phys.* **2007**, *126*, 074314-1−074314-11.

(10) Seibt, J.; Renziehausen, K.; Voronine, D. V.; Engel, V. Probing the Geometry Dependence of Molecular Dimers with Two-Dimensional Vibronic Spectroscopy. *J. Chem. Phys.* **2009**, *130*, 134318-1−134318-11.

(11) Schubert, A.; Renziehausen, K.; Engel, V. Mapping of Quantum Phases by Two-Dimensional Vibronic Spectroscopy of Wave-Packet Revivals. *Phys. Rev. A* **2010**, *82*, 013419-1−013419-4.

(12) Kjellberg, P.; Brüggemann, B.; Pullerits, T. Two-Dimensional Electronic Spectroscopy of an Excitonically Coupled Dimer. *Phys. Rev. B* **2006**, *74*, 024303-1−024303-9.

(13) Seibt, J.; Eisfeld, A. Intermolecular Torsional Motion of a π-Aggregated Dimer Probed by Two-Dimensional Electronic Spectroscopy. *J. Chem. Phys.* **2012**, *136*, 024109-1−024109-15.

(14) Panitchayangkoon, G.; Voronine, D. V.; Abramavicius, D.; Caram, J. R.; Lewis, N. H. C.; Mukamel, S.; Engel, G. S. Direct Evidence of Quantum Transport in Photosynthetic Light-Harvesting Complexes. *Proc. Natl. Acad. Sci. U.S.A.* **2011**, *108*, 20908−20912.

(15) Tiwari, V.; Peters, W. K.; Jonas, D. M. Electronic Resonance with Anticorrelated Pigment Vibrations Drives Photosynthetic Energy Transfer Outside the Adiabatic Framework. *Proc. Natl. Acad. Sci. U.S.A.* **2013**, *110*, 1203−1208.

(16) Christensson, N.; Kauffmann, H. F.; Pullerits, T.; Mančal, T. Origin of Long-Lived Coherences in Light-Harvesting Complexes. *J. Phys. Chem. B* **2012**, *116*, 7449−7454.

(17) Butkus, V.; Zigmantas, D.; Valkunas, L.; Abramavicius, D. Vibrational vs. Electronic Coherences in 2D Spectrum of Molecular Systems. *Chem. Phys. Lett.* **2012**, *545*, 40−43.

(18) Hamm, P. Three-dimensional-IR Spectroscopy: Beyond the Two-Point Frequency Fluctuation Correlation Function. *J. Chem. Phys.* **2006**, *124*, 124506-1−124506-13.

(19) Fidler, A. F.; Harel, E.; Engel, G. S. Dissecting Hidden Couplings Using Fifth-Order Three-Dimensional Electronic Spectroscopy. *J. Phys. Chem. Lett.* **2010**, *1*, 2876−2880.

(20) Turner, D. B.; Stone, K. W.; Gundogdu, K.; Nelson, K. A. Three-Dimensional Electronic Spectroscopy of Excitons in GaAs Quantum Wells. *J. Chem. Phys.* **2009**, *131*, 144510-1−144510-8.

(21) Kelley, A. M. Electron Phonon Coupling in CdSe Nanocrystals. *J. Phys. Chem. Lett.* **2010**, *1*, 1296−1300.

(22) Salvador, M. R.; Graham, M. W.; Scholes, G. D. Exciton-Phonon Coupling and Disorder in the Excited States of CdSe Colloidal Quantum Dots. *J. Chem. Phys.* **2006**, *125*, 880−886.

(23) Trallero-Giner, C.; Debernardi, A.; Cardona, M.; Menendez-Proupin, E.; Ekimov, A. I. Optical Vibrons in CdSe Dots and Dispersion Relation of the Bulk Material. *Phys. Rev. B* **1998**, *57*, 4664−4669.

(24) Nomura, S.; Kobayashi, T. Exciton-LO-Phonon Couplings in Spherical Semiconductor Microcrystallites. *Phys. Rev. B* **1992**, *45*, 1305−1316.

(25) Breuer, H.-P.; Petruccione, F. *Theory of Open Quantum Systems*; Oxford University Press: New York, 2002.

(26) Žídek, K.; Zheng, K.; Abdellah, M.; Lenngren, N.; Chábera, P.; Pullerits, T. Ultrafast Dynamics of Multiple Exciton Harvesting in the CdSe-ZnO System: Electron Injection versus Auger Recombination. *Nano Lett.* **2012**, *12*, 6393−6399.

(27) Žídek, K.; Zheng, K.; Ponseca, C. S.; Messing, M. E.; Wallenberg, L. R.; Chábera, P.; Abdellah, M.; Sundström, V.; Pullerits, T. Electron Transfer in Quantum-Dot-Sensitized ZnO Nanowires: Ultrafast Time-Resolved Absorption and Terahertz Study. *J. Am. Chem. Soc.* **2012**, *134*, 12110−12117.

(28) Sundström, V.; Pullerits, T.; van Grondelle, R. Photosynthetic Light-Harvesting: Reconciling Dynamics and Structure of Purple Bacterial LH2 Reveals Function of Photosynthetic Unit. *J. Phys. Chem. B* **1999**, *103*, 2327−2346.

(29) Turner, D. B.; Hassan, Y.; Scholes, G. D. Exciton Superposition States in CdSe Nanocrystals Measured Using Broadband Two-Dimensional Electronic Spectroscopy. *Nano Lett.* **2012**, *12*, 880−886.

(30) Pullerits, T.; Zigmantas, D.; Sundström, V. Beatings in Electronic 2D Spectroscopy Suggest Another Role of Vibrations in Photosynthetic Light Harvesting. *Proc. Natl. Acad. Sci. U.S.A.* **2013**, *110*, 1148−1149.

(31) Joe, Y. S.; Satanin, A. M.; Kim, C. S. Classical Analogy of Fano Resonances. *Phys. Scr.* **2006**, *74*, 259−266.

(32) Salvador, M. R.; Nair, P. S.; Cho, M.; Scholes, G. D. Interaction Between Excitons Determines the Non-linear Response of Nanocrystals. *Chem. Phys.* **2008**, *350*, 56−68.

(33) Christensson, N.; Milota, F.; Hauer, J.; Sperling, J.; Bixner, O.; Nemeth, A.; Kauffmann, H. F. High Frequency Vibrational Modulations in Two-Dimensional Electronic Spectra and Their Resemblance to Electronic Coherence Signatures. *J. Phys. Chem. B* **2011**, *115*, 5383−5391.

(34) Butkus, V.; Valkunas, L.; Abramavicius, D. Molecular Vibrations-Induced Quantum Beats in Two-Dimensional Electronic Spectroscopy. *J. Chem. Phys.* **2012**, *137*, 044513-1−044513-9.

(35) Pisliakov, A. V.; Mančal, T.; Fleming, G. R. Two-Dimensional Optical Three-Pulse Photon Echo Spectroscopy. II. Signatures of Coherent Electronic Motion and Exciton Population Transfer in Dimer Two-Dimensional Spectra. *J. Chem. Phys.* **2006**, *124*, 234505-1−234505-14.

(36) Kilina, S. V.; Kilin, D. S.; Prezhdo, V. V.; Prezhdo, O. V. Theoretical Study of Electron-Phonon Relaxation in PbSe and CdSe Quantum Dots: Evidence for Phonon Memory. *J. Phys. Chem. C* **2011**, *115*, 21641−21651.

(37) Madrid, A. B.; Hyeon-Deuk, K.; Habenicht, B. F.; Prezhdo, O. V. Phonon-Induced Dephasing of Excitons in Semiconductor Quantum Dots: Multiple Exciton Generation, Fission, and Luminescence. *ACS Nano* **2009**, *3*, 2487−2494.

(38) Kilina, S. V.; Kilin, D. S.; Prezhdo, O. V. Breaking the Phonon Bottleneck in PbSe and CdSe Quantum Dots: Time-Domain Density Functional Theory of Charge Carrier Relaxation. *ACS Nano* **2009**, *3*, 93−99.

(39) Mukamel, S. *Principles of Nonlinear Optical Spectroscopy*; Oxford University Press: New York, 1995.

(40) Norris, D. J.; Efros, A. L.; Rosen, M.; Bawendi, M. G. Size Dependence of Exciton Fine Structure in CdSe Quantum Dots. *Phys. Rev. B* **1996**, *53*, 16347−16354.

(41) Christensson, N.; Polivka, T.; Yartsev, A.; Pullerits, T. Photon Echo Spectroscopy Reveals Structure-Dynamics Relationships in Carotenoids. *Phys. Rev. B* **2009**, *79*, 245118-1−245118-14.
(42) Pullerits, T.; Monshouwer, R.; van Mourik, F.; van Grondelle, R. Temperature Dependence of Electron-Vibronic Spectra of Photosynthetic Systems. Computer Simulations and Comparison with Experiment. *Chem. Phys.* **1995**, *194*, 395−407.
(43) Uskov, A. V.; Jauho, A.-P.; Tromborg, B.; Mørk, J.; Lang, R. Dephasing Times in Quantum Dots due to Elastic LO Phonon-Carrier Collisions. *Phys. Rev. Lett.* **2000**, *85*, 1516−1519.
(44) Ishizaki, A.; Fleming, G. R. Unified Treatment of Quantum Coherent and Incoherent Hopping Dynamics in Electronic Energy Transfer: Reduced Hierarchy Equation Approach. *J. Chem. Phys.* **2009**, *130*, 234111-1−234111-10.
(45) Tanimura, Y. Stochastic Liouville, Langevin, Fokker-Planck, and Master Equation Approaches to Quantum Dissipative Systems. *J. Phys. Soc. Jpn.* **2006**, *75*, 082001-1−082001-39.
(46) Nalbach, P.; Ishizaki, A.; Fleming, G. R.; Thorwart, M. Iterative Path-Integral Algorithm versus Cumulant Time-Nonlocal Master Equation Approach for Dissipative Biomolecular Exciton Transport. *New J. Phys.* **2011**, *13*, 063040-1−063040-13.
(47) Egorova, D. Detection of Electronic and Vibrational Coherences in Molecular Systems by 2D Electronic Photon Echo Spectroscopy. *Chem. Phys.* **2008**, *347*, 166−176.
(48) Rodríguez-Suárez, R.; Menéndez-Proupin, E.; Trallero-Giner, C.; Cardona, M. Multiphonon Resonant Raman Scattering in Nanocrystals. *Phys. Rev. B* **2000**, *62*, 11006−11016.
(49) Tekavec, P. F.; Lott, G. A.; Marcus, A. H. Fluorescence-Detected Two-Dimensional Electronic Coherence Spectroscopy by Acousto-Optic Phase Modulation. *J. Chem. Phys.* **2007**, *127*, , 214307-1−214307-21.